JCTC Journal of Chemical Theory and Computation

ARTICLE

pubs.acs.org/JCTC

Enhanced Lipid Diffusion and Mixing in Accelerated Molecular Dynamics

Yi Wang,* Phineus R. L. Markwick, César Augusto F. de Oliveira, and J. Andrew McCammon

Center for Theoretical Biological Physics, Howard Hughes Medical Institute, Department of Chemistry and Biochemistry, Department of Pharmacology, University of California, San Diego, La Jolla, California 92093, United States

Supporting Information

ABSTRACT: Accelerated molecular dynamics (aMD) is an enhanced sampling technique that expedites conformational space sampling by reducing the barriers separating various low-energy states of a system. Here, we present the first application of the aMD method on lipid membranes. Altogether, ~1.5 μs simulations were performed on three systems: a pure POPC bilayer, a pure DMPC bilayer, and a mixed POPC:DMPC bilayer. Overall, the aMD simulations are found to produce significant speedup in *trans*−*gauche* isomerization and lipid lateral diffusion versus those in conventional MD (cMD) simulations. Further comparison of a 70-ns aMD run and a 300-ns cMD run of the mixed POPC:DMPC bilayer shows that the two simulations yield similar lipid mixing behaviors, with aMD generating a 2−3-fold speedup compared to cMD. Our results demonstrate that the aMD method is an efficient approach for the study of bilayer structural and dynamic properties. On the basis of simulations of the three bilayer systems, we also discuss the impact of aMD parameters on various lipid properties, which can be used as a guideline for future aMD simulations of membrane systems.

INTRODUCTION

Lipid bilayers are important components of cellular membranes. They serve as barriers against the diffusion of a large variety of biomolecules, thereby providing a structural basis of cellular compartmentalization. In recent years, molecular dynamics (MD) simulations have been increasingly used to study the dynamic properties of lipid bilayers.[1−12] For instance, the lateral diffusion coefficient, the rotation about the lipid long axis, and the collective undulatory motions have all been investigated in MD studies.[13−16] While these simulations have made a significant contribution to our understanding of lipid bilayers, the results are often compromised by the fact that dynamic behaviors at the lipid−water interface occur on time-scales that are not readily accessible to standard MD simulation approaches. For example, the lateral diffusion coefficient of lipids is on the order of 10^{-7} cm^2/s,[16] which means that on average a lipid molecule travels only ~10 Å in the bilayer plane during a 25-ns simulation. As a result, studying dynamic properties of complex membranes can become prohibitively expensive using atomistic MD simulations. This is exemplified by the mixing process of two or more types of lipids,[17−24] which generates mixed bilayers that better resemble cellular membranes than bilayers composed of a single lipid species.

In this study, we investigate the application of accelerated molecular dynamics (aMD)[25] to enhance the lateral diffusion and mixing of lipid molecules in a bilayer. In its original form, the aMD method modifies the potential energy landscape by adding a continuous, non-negative bias potential to the energy wells below a certain threshold, while leaving the energy barriers above this threshold unaffected.[25] As a result, barriers separating adjacent energy basins are reduced, allowing the system to sample conformational space with greater efficiency. Two parameters control the "amount" of acceleration introduced by aMD: the acceleration threshold energy E, which determines the portion of the energy surface affected by aMD, and the acceleration factor α, which determines how smooth the modified potential surface becomes.[25] The aMD method has been successfully applied in multiple studies of protein systems, such as GB3,[26] Ubiquitin,[27] Ras,[28] and the maltose binding protein.[29]

Here, we report the first application of aMD on lipid membranes, focusing on the effect of different aMD parameters on the *trans*−*gauche* isomerization, lateral diffusion, and mixing of a bilayer system. Simulations totaling ~1.5 μs were performed on three systems: a pure POPC bilayer, a pure DMPC bilayer, and a mixed POPC:DMPC bilayer. The two lipid species allow us to compare the effect of aMD on lipids with distinct properties: POPC has a saturated palmitoyl (16:0) chain and an unsaturated oleoyl chain (18:1), while DMPC has the saturated myristoyl (14:0) chain in both tails. We demonstrate that aMD can significantly enhance the *trans*−*gauche* isomerization and lateral diffusion for both lipid species. Furthermore, comparison with conventional MD (cMD) simulations reveals a significant speedup in lipid mixing in the aMD simulation of the POPC:DMPC bilayer. In the remainder of the text, we will first explain the design of the simulations and then discuss the results of the three systems mentioned above. Our results demonstrate that the aMD method is an efficient approach to studying lipid bilayers, which can also be extended to systems involving membrane proteins. The parameters examined in our simulations provide the first set of benchmarks for lipid aMD simulations, which may be used as a guideline for parameter selection in future aMD studies of membrane systems.

Received: June 22, 2011
Published: August 24, 2011

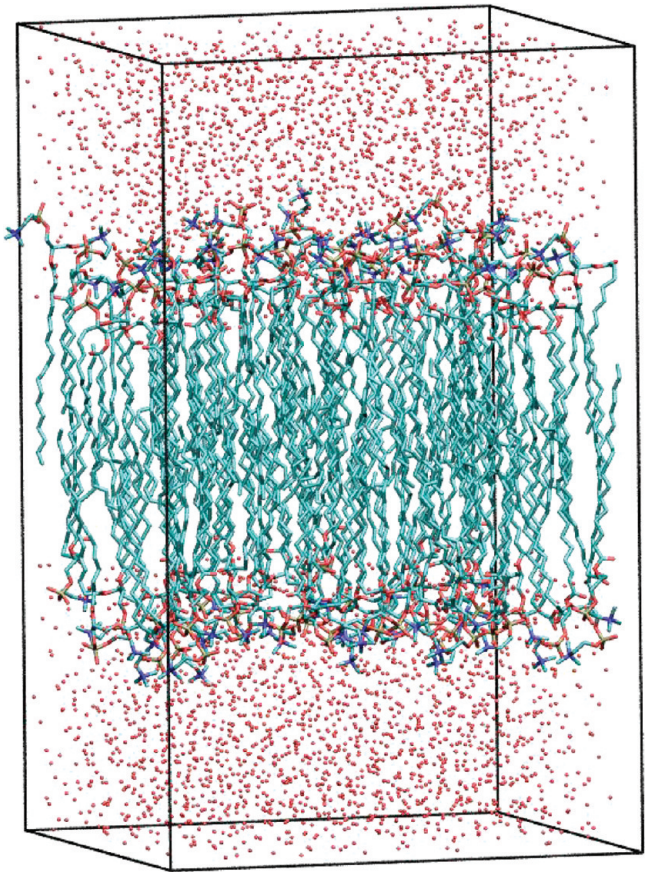

Figure 1. The initial structure of the POPC bilayer simulation system.

METHODS

System Preparation. A POPC bilayer was initially constructed using the *membrane* plugin of VMD[30] with 39 molecules in each leaflet. The membrane normal was placed along the z axis, and a 15-Å water layer was added to each side of the bilayer. The final system consists of 78 POPC molecules and 3693 water molecules. Since this study involves a comparative analysis of *trans*−*gauche* isomerization, the initial structure of the bilayer was designed to have a primarily *trans* conformation in the lipid tail region (Figure 1). However, simulating such a system directly under constant temperature and pressure (NPT) conditions results in erroneous artifacts, including significant interdigitation of the lipid tails and a considerable decrease in the bilayer thickness. Therefore, two test simulations were performed first, namely, a 1-ns simulation under constant temperature and volume (NVT) conditions, during which only the lipid tails were free to move, followed by a 10-ns NPAT (constant temperature, pressure, and surface area) simulation. The average volume of the system during the last nanosecond of the NPAT simulation was calculated and considered the target volume. Then, the following equilibration protocol was used to prepare the system for the production runs: Starting from the POPC system built initially (Figure 1), we performed a ∼10 ps NPT simulation with the phosphorus atoms constrained at their initial positions using a spring constant of 5 kcal/mol/Å^2, which was followed by a 20 ps NPAT run. These two short simulations brought the system to the target volume, while allowing most of the lipid tails to maintain their *trans* conformation. The final system has an area per lipid of 68.5 Å^2, which is similar to the experimentally determined value for POPC in the L_α phase (68.3 ± 1.5 Å^2).[31]

Table 1. cMD and aMD Simulations Performed for the POPC, DMPC, and Mixed POPC:DMPC Bilayers[a]

lipid	simulation	dE	$d\alpha$	t (ns)
POPC	cMD1			70
	cMD2			70
	E1	10	3	70
	E2a1	30	1	10
	E2a2	30	3	10
	E2a3	30	30	70
	E3a1	40	10	10
	E3a2	40	20	70
	E3a3	40	40	70
DMPC	cMD1			70
	cMD2			70
	E1	8.8	2.6	70
	E2a1	26.4	0.88	70
	E2a2	26.4	2.6	70
	E2a3	26.4	26.4	70
	E3a1	35.2	8.8	70
	E3a2	35.2	17.6	70
	E3a3	35.2	35.2	70
mix	cMD			300
	aMD	37.6	18.8	70

[a] The unit of aMD parameters (dE and $d\alpha$) is kcal/mol/lipid.

A DMPC bilayer was constructed using the above POPC bilayer as a template, which contained 78 DMPC molecules and 3535 water molecules. Following a protocol similar to that described above, this system was brought to the target volume with an area per lipid of 60.3 Å^2, comparable to the two reported experimental values for DMPC: 59.7 Å^2 [32] and 60.6 Å^2.[33] Additionally, a mixed bilayer was generated by combining half of the DMPC with half of the POPC system. The mixed bilayer contains 39 DMPC, 39 POPC, and 3532 water molecules, with an area per lipid of 64.9 Å^2.

aMD: The method. In the original form of aMD,[25] when the potential energy of the system falls below a threshold energy, E, a boost potential is added, such that the modified potential, $V^*(\mathbf{r})$, is related to the original potential, $V(\mathbf{r})$, via

$$V^*(\mathbf{r}) = V(\mathbf{r}) + \Delta V(\mathbf{r}) \quad (1)$$

where $\Delta V(\mathbf{r})$ is the boost potential

$$\Delta V(\mathbf{r}) = \begin{cases} 0 & V(\mathbf{r}) \geq E \\ \dfrac{(E - V(\mathbf{r}))^2}{\alpha + E - V(\mathbf{r})} & V(\mathbf{r}) < E \end{cases} \quad (2)$$

In the above equation, E is the threshold energy specified by the user, which controls the portion of the potential surface affected by the bias, and α is the acceleration factor that determines the shape of the modified potential: when E is fixed, the smaller α is, the more flattened the energy surface becomes.

From an aMD simulation, the ensemble average of an observable, $\langle A \rangle$, can be calculated via the following reweighting

equation:

$$\langle A \rangle = \frac{\langle A(\mathbf{r}) \exp(\beta \Delta V(\mathbf{r}))\rangle^*}{\langle \exp(\beta \Delta V(\mathbf{r}))\rangle^*} \quad (3)$$

in which $\beta = 1/k_B T$ and $\langle ... \rangle^*$ represents the ensemble average in the aMD ensemble.

aMD Simulation Parameters. Following the preparatory simulations described earlier, two cMD and seven aMD simulations were performed under NVT conditions for each of the POPC and DMPC bilayers (Table 1). All of the aMD simulations listed in Table 1 were performed using the "boosting dihedral" mode (aMDd).[25,34] Additionally, a dual-boost aMD (aMDdual)[35,36] simulation was performed for the POPC bilayer, which will be described in more detail in the Results and Discussion section. Similar to previous aMD studies,[27,37,35] the average dihedral energy of the system during a cMD simulation was used as a reference to set the aMD parameters E and α, *i.e.*, $E = V_{avg} + dE^*N$ and $\alpha = d\alpha^*N$, where V_{avg} is the average dihedral energy of the system in the first 1 ns of the cMD simulation, $N = 78$ is the number of lipid molecules, and dE and $d\alpha$ are constants with units of kcal/mol/lipid. For the pure POPC bilayer, three acceleration threshold energy values (E1, E2, and E3) were examined, with $dE = 10$, 30, and 40 kcal/mol/lipid, respectively. For the last two acceleration thresholds, three independent simulations were performed with different α values (a1, a2, and a3). Note that while E1, E2, and E3 uniquely identify the threshold energy used in an aMD simulation, a1, a2, and a3 only distinguish simulations within the same threshold energy level, *i.e.*, E2a2 and E3a2 have different α values (see Table 1).

In order to keep the acceleration level comparable for the POPC and DMPC bilayers, the aMD parameters for the pure DMPC bilayer were set using the same equations described above, with dE and $d\alpha$ scaled by $\text{dihe}_{DMPC}/\text{dihe}_{POPC}$, *i.e.*, the ratio of the number of dihedrals in the DMPC and POPC bilayers.

With the exception of three POPC aMD runs, all cMD and aMD simulations mentioned above were performed for 70 ns. Three POPC aMD simulations, E2a1, E2a2, and E3a1, revealed artificial *cis*−*trans* conformational changes and were terminated at $t = 10$ ns. These simulations are discussed in more detail in the Results and Discussion section. Following each 70-ns aMD run, a 10-ns cMD simulation was performed, the starting structure of which was taken from the snapshot with the highest boost potential in the last 5 ns of the aMD trajectory. We will refer to them as "-eq" trajectories of the corresponding aMD runs; *e.g.*, E1-eq refers to the 10-ns cMD simulation following the aMD run E1.

For the mixed POPC:DMPC bilayer, one cMD and one aMD simulation were performed. The aMD parameters were chosen on the basis of the E3a2 simulations of POPC and DMPC (see Table 1). The aMD simulation of the mixed bilayer was performed for 70 ns, while the cMD simulation was performed for 300 ns to allow sufficient lipid mixing events to be sampled.

Simulation Protocols. As this study was initiated before the latest CHARMM36 force field[38] was available, the CHARMM27r force field for lipids was used.[39,40] The cMD simulations were performed with the 2.7b1 release of NAMD,[41] while the aMD simulations were performed with the recent NAMD implementation of aMD,[34] now availabe in the 2.8 release of the software. All simulations were performed using a time step of 2 fs, with bonds involving hydrogen atoms constrained using RATTLE[42] and water geometries maintained using SETTLE.[43] The multiple-time-stepping algorithm was used, with short-range forces calculated every step and long-range electrostatics calculated every 2 steps. The cutoff for short-range nonbonded interactions was set to 12 Å, with a switching distance of 10 Å. Assuming periodic boundary conditions, the particle mesh Ewald (PME) method[44] with a grid density of at least $1/\text{Å}^3$ was employed for computation of long-range electrostatic forces. The temperature was maintained at 303 K for all simulations using Langevin dynamics with a damping coefficient of 1 ps^{-1}. In NPT or NPAT simulations, the pressure was kept constant at 1 atm using a Nosé−Hoover−Langevin piston.[45]

RESULTS AND DISCUSSION

Performance of aMD. In line with a previous study,[34] the aMD simulations performed with NAMD are slightly slower than the corresponding cMD runs. Using a local cluster with InfiniBand connections, the cMD and aMD simulations gave on average 0.0758 days/ns and 0.0782 days/ns on 36 processors or 0.0624 days/ns and 0.0680 days/ns on 48 processors, respectively. The 3−9% slowdown in aMD is primarily due to an extra round of energy reduction calls.[34] More comprehensive evaluation of the aMD performance can be found in the aforementioned study.

Pure POPC and DMPC Bilayers. *trans/gauche Ratio.* For both POPC and DMPC bilayers, the probability distributions of the lipid tail dihedrals were constructed using the last 20 ns of the 70-ns cMD simulations. Since the *trans*−*gauche* isomerization is a rapid process, the above results can be viewed as equilibrium distribution profiles. As shown in Figure S1 (Supporting Information), most dihedrals exhibit similar distributions, with three notable exceptions in the POPC bilayer: C7−C8−C9−C10, C8−C9−C10−C11, and C9−C10−C11−C12, which all involve the *cis* double bond in the unsaturated oleoyl chain. On the basis of the profiles in Figure S1, we calculated the *trans*/*gauche* ratio with the *trans* conformation defined as $\chi \leq -150°$ or $\chi > 150°$ and the *gauche* conformation defined as $-97° < \chi \leq -37°$ or $37° < \chi \leq 97°$. Due to their unique distribution profiles, the three dihedrals mentioned above are not included in the calculation of the *trans*/*gauche* ratio for POPC.

As shown in Figure S2 (Supporting Information), while the simulations started with a primarily *trans* conformation, the *trans*/*gauche* ratio became stabilized shortly after the simulations began. This fast isomerization is consistent with results from earlier studies.[46] To quantify the difference between cMD and aMD results, we calculated the equilibrium *trans*/*gauche* ratio using the last 20 ns of each cMD and aMD run and recorded the time when a simulation first reached its equilibrium value. Overall, the isomerization appears to be slower in POPC than DMPC: The equilibrium *trans*/*gauche* ratio was reached in 526 and 727 ps in the two cMD simulations of POPC, while the corresponding numbers are 55 and 82 ps in the two cMD simulations of DMPC. For both lipid species, aMD produced a significant speedup, with the fastest isomerization occurring within 81 ps for POPC and 13 ps for DMPC, corresponding to a 7.7- and 5.3-fold speedup from the cMD simulations, respectively. The slower isomerization in POPC may be related to its longer hydrocarbon tails and a lower equilibrium *trans*/*gauche* ratio (2.08) than DMPC (2.44). It should be noted that since the simulations started with the area per lipid corresponding to an L_α-phase bilayer, these results only reflect the difference

of cMD and aMD in promoting *trans*−*gauche* isomerization and should not be compared to a gel-to-fluid phase transition.

Lateral Diffusion Coefficient. The lipid lateral diffusion coefficient D was calculated according to the Einstein relation:

$$D = \frac{1}{N}\sum_{i}^{N}\frac{1}{4t}\langle|\mathbf{r}_i(t) - \mathbf{r}_i(0)|^2\rangle \quad (4)$$

where N is the number of lipids in the system, $\mathbf{r}_i(t)$ and $\mathbf{r}_i(0)$ are the coordinates of the center-of-mass (COM) of a lipid molecule in the membrane plane at time t and time 0, respectively. To allow for sufficient equilibration, the last 60 ns of each cMD and aMD simulation were used to calculate D. The time origin $t = 0$ was shifted along the simulation trajectory to make use of all data points, and the mean square displacement (MSD) data from $t = 1$ ns to $t = 20$ ns were used to determine D by a least-squares method.

The lateral diffusion coefficients obtained from the above calculations are listed in Table 2. To quantify the comparison of cMD and aMD results, we took the average of D obtained from the two cMD simulations of each bilayer and used it to calculate the relative lateral diffusion coefficients (D_{relative}) for each simulation. As shown in Figure 2 and Table 2, significant speedup is observed in all aMD simulations, with a maximum speedup of 247% for POPC and 287% for DMPC in the aMDd runs. Furthermore, a 349% speedup is observed in the aMDdual simulation of POPC. The difference in the two lipid species and the effect of aMD parameters on lipid lateral diffusion are discussed in the next section.

Table 2. Lateral Diffusion Coefficients of POPC and DMPC Calculated from cMD and aMD Simulations[a]

	POPC		DMPC	
simulation	D (10^{-8} cm^2/s)	D_{relative}	D (10^{-8} cm^2/s)	D_{relative}
cMD1	6.2	98%	6.4	107%
cMD2	6.4	102%	5.5	93%
E1	10.4	164%	8.9	149%
E2a1			17.2	287%
E2a2			12.6	212%
E2a3	15.6	247%	9.1	152%
E3a1			17.0	285%
E3a2	15.2	240%	13.9	233%
E3a3	10.8	172%	10.8	181%

[a] D_{relative} is defined as $2D/(\text{D1} + \text{D2})$, where D1 and D2 are the diffusion coefficients of the cMD1 and cMD2 simulations, respectively.

Recently, Roark and Feller[16] showed that for a small system, the correlation length of monolayer COM motions was comparable with the dimension of the simulation unit cell. As a result, a small system may produce an artificially large D.[7] Removing the monolayer COM prior to the calculation alleviates this problem, although such a treatment also introduces another artifact,[47] resulting in the underestimation of the lateral diffusion coefficient.[16] In this study, the monolayer COM motions are removed before the calculation of D, because it produces the highest statistical precision for our simulation data (see Figure S3, Supporting Information). While we note that this treatment still suffers from the finite size effect described by Yeh and Hummer,[47] such an effect is present in both cMD and aMD simulations and, therefore, should not affect the comparison of the two methods significantly.

Effect of E and α. Further analysis of the lateral diffusion coefficients allows us to examine the effect of aMD parameters: Overall, larger values of E and smaller values of α produce faster lateral diffusion, which is explained by a higher boost potential as a result of the changes in E and α. For instance, with dE kept at 40 kcal/mol/lipid, decreasing $d\alpha$ from 40 (E3a3) to 20 (E3a2) kcal/mol/lipid increased the POPC lateral diffusion coefficient by 40%. Meanwhile, with $d\alpha$ kept at 2.6 kcal/mol/lipid, increasing dE from 8.8 (E1) to 26.4 (E2a2) kcal/mol/lipid for DMPC increased D by 42%. Such a general relationship between the acceleration level and the two aMD parameters has been well established in earlier aMD studies of peptides or proteins.[25,26,34,48]

Comparison of the DMPC E1 and all of the E3 simulations suggests that the parameter E plays the dominant role in these aMD runs, since the increase in E determines the speedup in lipid lateral diffusion. Similar observations can be made from the comparison of E1 and E2a3 simulations of POPC. These results

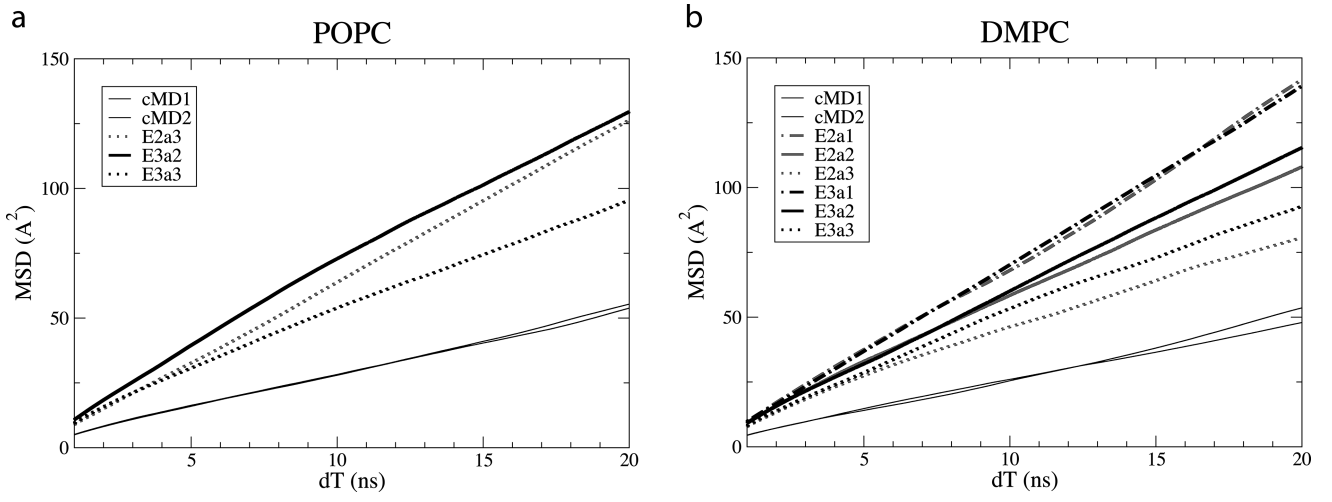

Figure 2. The mean square displacement (MSD) of POPC (a) and DMPC (b) calculated from cMD and aMD simulations. The cMD results are shown in thin black lines, while the aMD results are shown in thick lines. Results from different aMD simulations are distinguished by their colors and line styles. The corresponding lateral diffusion coefficients are listed in Table 2.

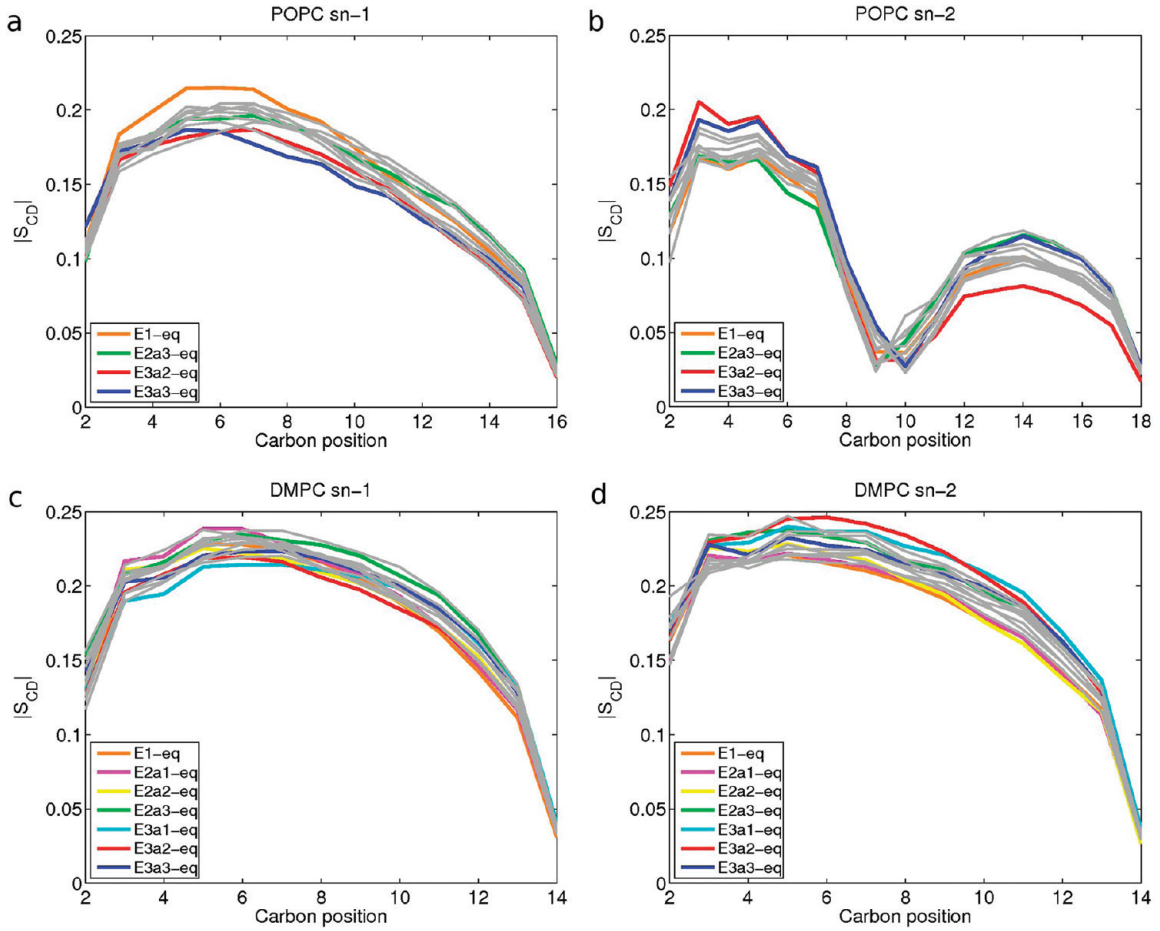

Figure 3. Order parameter S_{CD} of POPC (a, b) and DMPC (c, d) in aMD-eq simulations. Calculations were performed using the last 5 ns of the 10-ns aMD-eq simulations (colored lines). For comparison, the same calculation was repeated using a 5-ns block for the last 20 ns of the cMD1 and cMD2 simulations (eight gray lines).

suggest that when the initial acceleration threshold energy is low, increasing E is very efficient in raising the acceleration level. However, once E becomes large, α often assumes the dominant role in determining the speedup of the lateral diffusion. For example, when dE is reduced from 40 (E3a3) to 30 (E2a3) kcal/mol/lipid, decreasing α still results in larger D for POPC, suggesting that the impact of α outweighs that of E in these cases.

The analysis of all aMD simulations listed in Table 1 reveals that POPC is more sensitive to the change in α than DMPC. This difference may be explained by the different structures of the two lipids: the double bond in the sn-2 oleoyl chain of POPC produces a large energy barrier, which is smoothened by small α values. Such a role of α in controlling the roughness of the modified potential[49,50] and the dynamics of the simulated system has been investigated in previous studies.[35,51] In the case of POPC, when α becomes too small, the energy barrier of the double bond is significantly lowered, and the artificial *cis*−*trans* transition may occur. Such an artifact (Figure S4, Supporting Information) is observed in three aMD simulations, E2a1, E2a2, and E3a1, where $d\alpha$ was set to 1, 3, and 10 kcal/mol/lipid, respectively. These aMD simulations were terminated at $t = 10$ ns and not included in any further analysis. Apart from simulations designed to study the double bond *cis*−*trans* transition, small α values should be used with caution to avoid similar artifacts in aMD simulations of unsaturated fatty acids.

Another interesting observation from Figure 2 is that once the acceleration has been raised to a certain level, either through increasing E or decreasing α, the effect of further acceleration can be very limited. For instance, while the POPC E3a2 simulation has the largest E and the smallest α, its lateral diffusion coefficient is very similar to E2a3, which has the second highest acceleration level among aMD simulations of POPC. This result may reflect the limit of the aMD method used in these simulations, where only the dihedral potential is boosted (the aMDd mode). The speedup observed in these simulations may be attributed to a more flexible lipid structure, as revealed by the faster *trans*−*gauche* isomerization of lipid tails (Figure S2, Supporting Information) and increased rotation and barrier-crossing events of the headgroup (Figure S5, Supporting Information). Since nonbonded interactions are known to play an important role in bilayer dynamics, the lipid lateral diffusion can be expected to be further enhanced using aMDT (boosting the total potential) or aMDdual (dual boost) simulations, where the boost potential is applied to all degrees of freedom in the system.[35,36] As a test of this hypothesis, we performed an aMDdual simulation on the POPC bilayer (Figure S6, Supporting Information), where the same boost potential used in the E3a2 simulation was chosen for the dihedrals, with a separate boost potential ($dE = d\alpha = 0.15$ kcal/mol/atom, see Figure S6) applied on the remaining

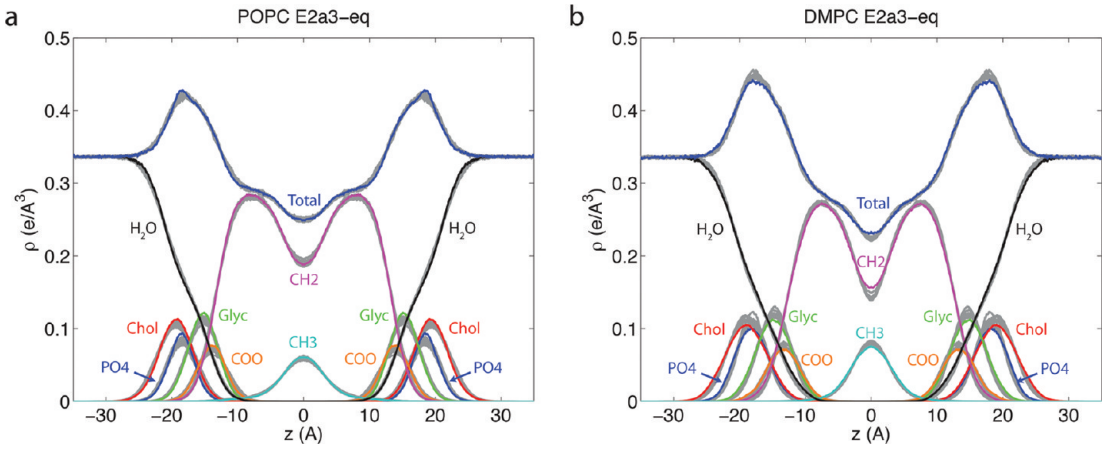

Figure 4. Electron density profiles of POPC (a) and DMPC (b) in selected aMD-eq simulations. Calculations were performed using the last 5 ns of the 10-ns aMD-eq simulations (colored lines). For comparison, the same calculations were repeated using a 5-ns block for the last 20 ns of the cMD1 and cMD2 simulations (eight gray lines).

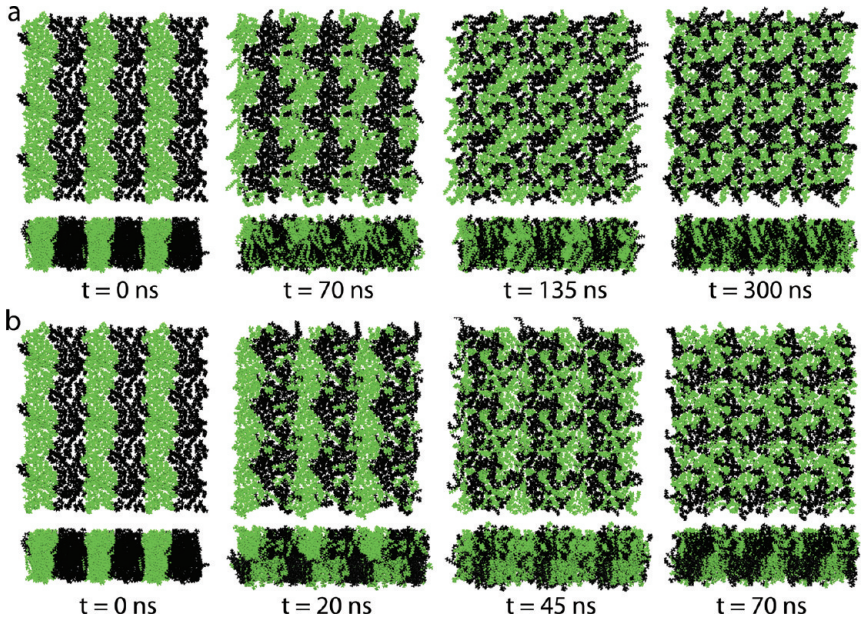

Figure 5. Representative snapshots of the mixed POPC:DMPC bilayer in cMD (a) and aMD (b) simulations. The POPC and DMPC molecules are colored in black and green, respectively. For clarity, only one monolayer is displayed in the top view figures, and nine periodic images, including the original unit cell in the middle, are shown. Both monolayers are included in the side view figures, and three periodic images are shown.

degrees of freedom. As shown in Figure S6, the lateral diffusion is enhanced by an additional 45% relative to the E3a2 simulation described earlier. Further optimization of the aMD parameters may lead to an even greater speedup and is currently under investigation in our lab.

Equilibration of aMD Systems. As shown in Figure S2 (Supporting Information), the *trans/gauche* ratios obtained from aMD simulations are slightly different from the corresponding cMD results. Indeed, the equilibrium *trans/gauche* ratio ranges from 1.90 to 2.04 in the POPC aMD simulations and from 1.98 to 2.31 in the DMPC aMD simulations, while the corresponding cMD values, averaged over cMD1 and cMD2, are 2.08 for POPC and 2.44 for DMPC. Such differences are expected for these unweighted aMD simulations, since the ensemble average of an observable needs to be recovered from the reweighting procedure given in eq 3. Unfortunately, straightforward application of eq 3 remains a challenge for systems with tens of thousands of atoms, due to the statistical noise associated with the exponential form of the reweighting equation, which tends to manifest any small fluctuations in the boost potential.[52]

In this work, we explored the use of a short cMD simulation to bring the aMD system back to the original, unbiased ensemble. As described in the Methods section, we performed a 10-ns cMD simulation seeded from the structure with the highest boost potential in the last 5 ns of an aMD trajectory. The high boost potential determines that the corresponding structure has a relatively large weight in the reweighting process. From the aMD-eq simulations, we calculated various structural properties of the bilayer, including the order parameter S_{CD} and the electron

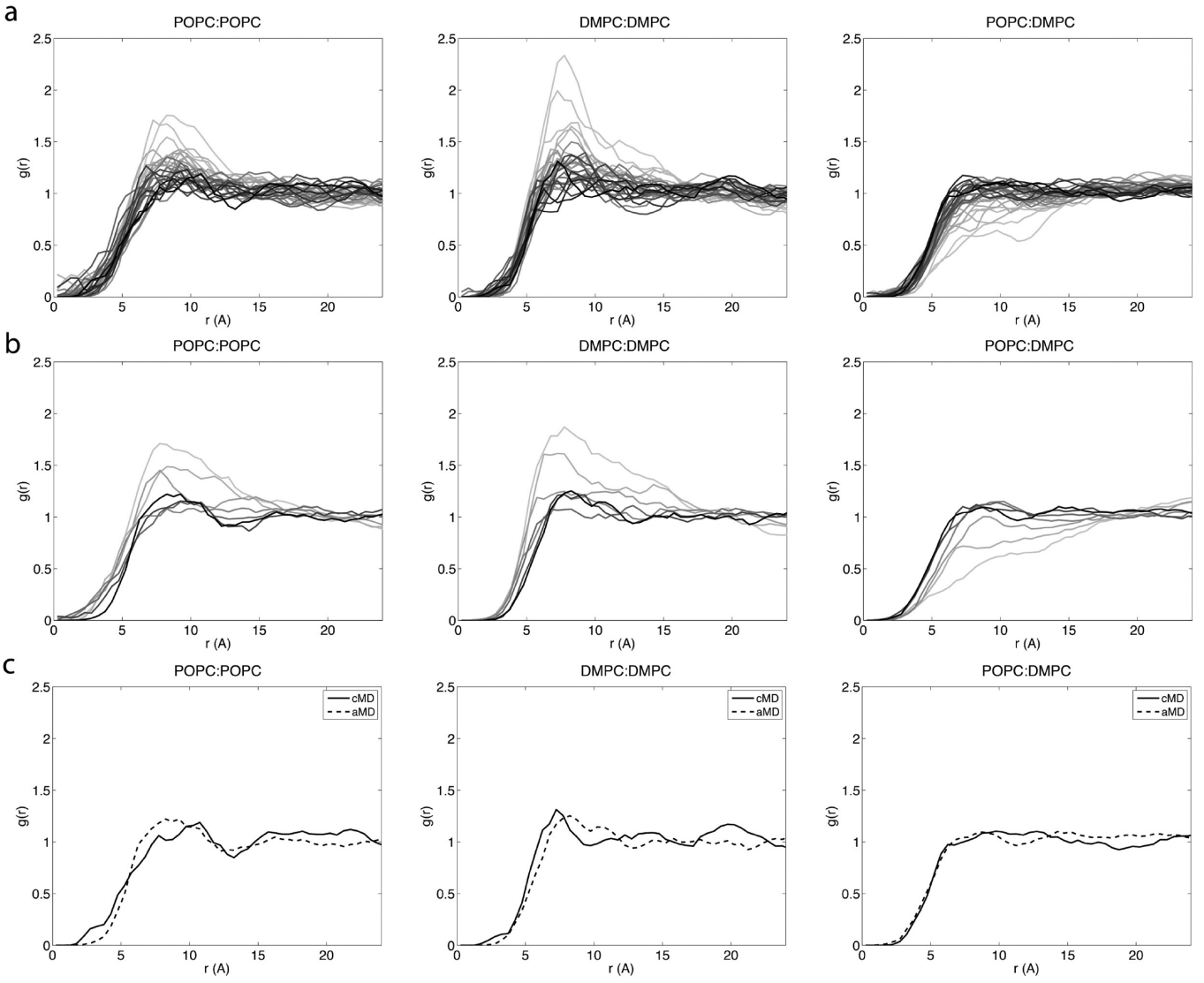

Figure 6. Radial pair distribution functions of the mixed POPC:DMPC bilayer. (a, b) Results of the cMD (a) and aMD (b) simulations. The $g(r)$ calculations were performed using a 10-ns block for three lipid pairs—POPC:POPC, DMPC:DMPC, and POPC:DMPC. Results are colored in light gray for the beginning of a simulation and dark gray for the end of the simulation. (c) Comparison of $g(r)$ obtained from the last 10 ns of the cMD (solid line) and aMD (dashed line) simulations.

density profile (EDP). By comparing these properties with results from the 70-ns cMD simulations, we evaluated the ability of the aMD-eq simulations to bring the bilayer systems to the original potential energy surface.

The deuterium order parameter S_{CD}, which is a measure of the disorder in lipid tails, was calculated from our simulations according to

$$S_{CD} = \frac{1}{2}\langle 3\cos^2\theta - 1\rangle \quad (5)$$

where θ is the angle between the CH-bond vector and the bilayer normal. The electron density profile EDP was obtained according to Feller et al.;[53] namely, the time-averaged number of electrons was counted for every 0.1-Å slab along the membrane normal. As shown in Figures 3 and 4, overall, the S_{CD} and EDP calculated from the aMD-eq simulations are very similar with the cMD results. A slightly larger deviation is observed for the S_{CD} of the POPC sn-2 chain in the E3a2-eq simulation (Figure 3). In light of this deviation, we extended the E3a2-eq run to 20 ns and repeated the S_{CD} calculations. As shown in Figure S7 (Supporting Information), the S_{CD} results of the extended simulation agree well with the cMD data. Additionally, we also found good agreement between aMD-eq and cMD results for the distribution profiles of all headgroup dihedrals, as well as the equilibrium *trans*−*gauche* ratios of lipid tails (data not shown).

On the basis of the above analysis, we conclude that the 10-ns aMD-eq simulations allowed most bilayer systems to relax back to the original, unbiased ensemble. However, since longer equilibration was required for the E3a2 simulation of POPC, these results also suggest that aggressive acceleration levels should be used with caution, since they might render undesirable structural artifacts or require longer equilibrations following aMD. Overall, the relatively short equilibrations described above suggest that our bilayers were not driven too far away from the original ensemble by the aMD boost potential. This result may be attributed to the relatively modest acceleration applied in the

current study, as well as the homogeneous nature of a lipid bilayer, which tends to have a smoother potential surface compared with protein systems. A number of studies have investigated post-aMD analysis methods for protein systems[28,29,54] and the reweighting issue described earlier.[55,56]

Mixing of POPC and DMPC. Encouraged by the enhanced lipid lateral diffusion in aMD simulations, we set out to examine the effect of aMD on lipid mixing. On the basis of the lateral diffusion calculation described above, we set the acceleration level to dE = 37.6 kcal/mol/lipid and $d\alpha$ = 18.8 kcal/mol/lipid, equivalent to the E3a2 simulations of pure POPC or DMPC, which produced the best performance in enhancing lipid diffusion without affecting the conformation of the POPC sn-2 chain.

As shown in Figure 5, the mixing of POPC and DMPC is significantly expedited by the aMD simulation. To quantify the comparison, we calculated the 2D radial distribution functions, $g(r)$, for the lipid pairs DMPC:DMPC, POPC:POPC, and POPC:DMPC. The calculation was performed for each monolayer separately, using the projection of lipid COMs on the membrane plane. The evolution of $g(r)$ in both cMD and aMD simulations is highlighted by the color change from light gray to dark gray in Figure 6. As clearly shown in this figure, during both simulations, the $g(r)$ peak at r = 8−10 Å in the DMPC:DMPC and POPC:POPC pair distribution functions is gradually smoothened, indicating that the lipid molecules are no longer characterized by the clustering of like neighbors. The $g(r)$ of the POPC:DMPC pair has an opposite trend, which corresponds to an increasing degree of mixing. Note that the final $g(r)$ functions are very similar in the two simulations (Figure 6c), which indicates that the aMD result is in good agreement with the cMD simulation.

Analysis of the $g(r)$ data shows that the lipids are well mixed at t = 50 ns in the aMD simulation, which is reflected in a small (0.21) root-mean-square-deviation (RMSD) of the POPC:DMPC $g(r)$ compared to the final $g(r)$. In contrast, the RMSD of the POPC:DMPC $g(r)$ is 0.77 at t = 70 ns in the cMD simulation and only dropped to 0.29 at t = 120 ns. Similarly, with reference to the final DMPC:DMPC $g(r)$, the RMSD of the aMD run reached 0.33 at t = 40 ns, while the RMSD of the cMD run is 0.43 at t = 130 ns. On the basis of these results, we estimate that aMD affords an approximate 2−3-fold speedup in lipid mixing compared to the cMD simulation.

Interestingly, both the cMD and aMD results suggest that the POPC:DMPC bilayer may deviate from an ideal mixture, which is in agreement with phase diagrams derived from calorimetric data.[57,58] As shown in Figure 5, small clusters of like lipids can be identified at the end of both aMD and cMD simulations. Meanwhile, the $g(r)$ plots revealed a small peak at r = 8−10 Å in the final DMPC:DMPC and POPC:POPC radial distribution functions, which is absent in the POPC:DMPC result (Figure 6c). These data reflect a tendency for lipids of the same species to aggregate in the mixed POPC:DMPC bilayer, which may be explained by nonideal mixing of the bilayer. However, even for an ideal mixture, the system is likely to experience fluctuations and occasionally deviate from ideality. Therefore, cMD or aMD simulations of longer duration are needed to fully understand the mixing behaviors of the POPC:DMPC system at the atomistic level. Given the lateral diffusion results discussed earlier, larger bilayers of mixed lipid species may be used to reduce the finite size effect.[47] The computational resources conserved through the use of aMD may be even greater for these larger bilayers, since the cost of a simulation is proportional to the size of the system.

CONCLUSIONS

Using 1.5-μs simulations, we studied the effect of accelerated MD on *trans*−*gauche* isomerization, lateral diffusion, and lipid mixing of three bilayer systems—POPC, DMPC, and mixed POPC:DMPC. Overall, aMD produced a significant speedup in lipid equilibration and diffusion: For the pure POPC and DMPC bilayers, aMD produced up to 8 times faster *trans*−*gauche* isomerization and up to a 3-fold speedup in lipid lateral diffusion. From a comparative analysis of seven aMD simulations for each of the POPC and DMPC bilayers, we examined the effect of aMD parameters on the structural and dynamic properties of the two lipid species. POPC was found to be more sensitive to the acceleration factor α, which controls the shape of the modified potential energy surface. We demonstrate that small α values can produce significant speedup in lipid lateral diffusion. However, on further decreasing α below a certain threshold, the artificial *cis*−*trans* transition may occur in the POPC oleoyl chain, due to the smoothened energy barrier associated with the double bond. For this reason, α should be chosen with caution to avoid such an artifact in aMD simulations of unsaturated lipids. Meanwhile, selective aMD,[56] where the boost potential is only applied to a certain part of the system, may prove a useful alternative for these systems.

On the basis of the results of pure POPC and DMPC bilayers, we tested the ability of aMD to enhance lipid mixing in the POPC:DMPC bilayer. A 70-ns aMD simulation and a 300-ns cMD run revealed similar mixing behaviors, with aMD producing a 2−3-fold increase in the mixing speed. Since interactions with lipids are crucial to the stability and proper function of a large number of membrane proteins, the aMD method may be particularly useful in speeding up the equilibration of various lipid species surrounding a membrane protein. The results presented in this work provide the benchmarks for these future aMD studies of bilayers with single- or multiple-lipid components. Additionally, the parameters examined here can be used as a starting point for further optimization in aMD simulations of membrane systems.

ASSOCIATED CONTENT

Supporting Information. Probability distribution of lipid tail dihedrals (Figure S1), the *trans/gauche* ratio (Figure S2), the mean square displacement of lipid molecules (Figure S3), the conformations of the sn-2 oleoyl chain in POPC (Figure S4), barrier-crossing events (Figure S5), and the mean square displacement in dual-boost aMD simulation (Figure S6). This information is available free of charge via the Internet at http://pubs.acs.org/

AUTHOR INFORMATION

Corresponding Author
*E-mail: yiwang@ucsd.edu.

ACKNOWLEDGMENT

We thank Dr. Richard Pastor for suggesting the lipid mixing simulations. This work has been supported in part by the National Science Foundation, the National Institutes of Health,

Howard Hughes Medical Institute, Center for Theoretical Biological Physics, the National Biomedical Computation Resource, and the NSF supercomputer centers. The authors appreciate the computational resources provided by the Texas Advanced Computing Center (TG-MCA93S013 and TG-MCB090187).

REFERENCES

(1) Feller, S. E. *Curr. Opin. Colloid Interface Sci.* **2000**, *5*, 217–223.
(2) Saiz, L.; Bandyopadhyay, S.; Klein, M. L. *BSR* **2002**, *22*, 151–173.
(3) Pastor, R. W.; Venable, R. M.; Feller, S. E. *Acc. Chem. Res.* **2002**, *35*, 438–446.
(4) Lopez, C.; Moore, P.; Shelley, J.; Shelley, M.; Klein, M. *Comput. Phys. Commun.* **2002**, *147*, 1–6.
(5) McWhirter, J. L.; Ayton, G.; Voth, G. A. *Biophys. J.* **2004**, *87*, 3242–3263.
(6) Ayton, G. S.; Voth, G. A. *Biophys. J.* **2004**, *87*, 3299–3311.
(7) Klauda, J.; Brooks, B.; Pastor, R. *J. Chem. Phys.* **2006**, *125*, 144710.
(8) Klauda, J.; Kucerka, N.; Brooks, B.; Pastor, R.; Nagle, J. *Biophys. J.* **2006**, *90*, 2796–2807.
(9) Izvekov, S.; Voth, G. A. *J. Chem. Theory Comput.* **2006**, *2*, 637–648.
(10) Marrink, S. J.; Risselada, H. J.; Yefimov, S.; Tieleman, D. P.; de Vries, A. H. *J. Phys. Chem. B* **2007**, *111*, 7812–7824.
(11) Berkowitz, M. *Biochim. Biophys. Acta* **2009**, *1788*, 86–96.
(12) Falck, E.; Róg, T.; Karttunen, M.; Vattulainen, I. *J. Am. Chem. Soc.* **2008**, *130*, 44–45.
(13) Lindahl, E.; Edholm, O. *Biophys. J.* **2000**, *79*, 426–433.
(14) Saiz, L.; Klein, M. L. *Acc. Chem. Res.* **2002**, *35*, 482–489.
(15) Pitman, M. C.; Suits, F.; Gawrisch, K.; Feller, S. E. *J. Chem. Phys.* **2005**, *122*, 244715.
(16) Roark, M.; Feller, S. E. *J. Phys. Chem. B* **2009**, *113*, 13229–13234.
(17) Huang, J.; Swanson, J.; Dibble, A.; Hinderliter, A.; Feigenson, G. *Biophys. J.* **1993**, *64*, 413–425.
(18) Chiu, S.; et al. *Biophys. J.* **1999**, *77*, 2462–2469.
(19) Smondyrev, A.; Berkowitz, M. *Biophys. J.* **1999**, *77*, 2075–2089.
(20) Sugár, I. P.; Thompson, T. E.; Biltonen, R. L. *Biophys. J.* **1999**, *76*, 2099–2110.
(21) Pandit, S.; Bostick, D.; Berkowitz, M. *Biophys. J.* **2004**, *86*, 1345–1356.
(22) Zhang, Z.; Bhide, S.; Berkowitz, M. *J. Phys. Chem. B* **2007**, *111*, 12888–12897.
(23) Coppock, P. S.; Kindt, J. T. *Langmuir* **2009**, *25*, 352–359.
(24) Yin, F.; Kindt, J. T. *J. Phys. Chem. B* **2010**, *114*, 8076–8080.
(25) Hamelberg, D.; Mongan, J.; McCammon, J. *J. Chem. Phys.* **2004**, *120*, 11919–11929.
(26) Markwick, P.; Bouvignies, G.; Blackledge, M. *J. Am. Chem. Soc.* **2007**, *129*, 4724–4730.
(27) Markwick, P.; Bouvignies, G.; Salmon, L.; McCammon, J.; Nilges, M.; Blackledge, M. *J. Am. Chem. Soc.* **2009**, *131*, 16968–16975.
(28) Grant, B.; Gorfe, A.; McCammon, J. *PLoS Comput. Biol.* **2009**, *5*, e1000325.
(29) Bucher, D.; Grant, B.; Markwick, P.; McCammon, J. *PLoS Comput. Biol.* **2011**, *7*, e1002034.
(30) Humphrey, W.; Dalke, A.; Schulten, K. *J. Mol. Graphics* **1996**, *14*, 33–38.
(31) Kucerka, N.; Tristram-Nagle, S.; Nagle, J. F. *J. Membr. Biol.* **2005**, *208*, 193–202.
(32) Petrache, H. I.; Tristram-Nagle, S.; Nagle, J. F. *Chem. Phys. Lipids* **1998**, *95*, 83–94.
(33) Kucerka, N.; Liu, Y.; Chu, N.; Petrache, H. I.; Tristram-Nagle, S.; Nagle, J. F. *Biophys. J.* **2005**, *88*, 2626–2637.
(34) Wang, Y.; Harrison, C. B.; Schulten, K.; McCammon, J. A. *Comput. Sci. Discovery* **2011**, *4*, 015002.
(35) de Oliveira, C.; Hamelberg, D.; McCammon, J. *J. Phys. Chem. B* **2006**, *110*, 22695–22701.
(36) Hamelberg, D.; de Oliveira, C.; McCammon, J. *J. Chem. Phys.* **2007**, *127*, 155102.
(37) Hamelberg, D.; Shen, T.; McCammon, J. *J. Am. Chem. Soc.* **2005**, *127*, 1969–1974.
(38) Klauda, J. B.; Venable, R. M.; Freites, J. A.; O'Connor, J. W.; Tobias, D. J.; Mondragon-Ramirez, C.; Vorobyov, I.; MacKerell, A. D., Jr.; Pastor, R. W. *J. Phys. Chem. B* **2010**, *114*, 7830–7843.
(39) Klauda, J.; Brooks, B.; MacKerell, A. D.; Venable, R.; Pastor, R. *J. Phys. Chem. B* **2005**, *109*, 5300–5311.
(40) Klauda, J.; Pastor, R.; Brooks, B. *J. Phys. Chem. B* **2005**, *109*, 15684–15686.
(41) Phillips, J. C.; Braun, R.; Wang, W.; Gumbart, J.; Tajkhorshid, E.; Villa, E.; Chipot, C.; Skeel, R. D.; Kale, L.; Schulten, K. *J. Comput. Chem.* **2005**, *26*, 1781–1802.
(42) Andersen, H. C. *J. Chem. Phys.* **1983**, *52*, 24–34.
(43) Miyamoto, S.; Kollman, P. A. *J. Comput. Chem.* **1993**, *13*, 952–962.
(44) Darden, T.; York, D.; Pedersen, L. *J. Chem. Phys.* **1993**, *98*, 10089–10092.
(45) Feller, S. E.; Zhang, Y. H.; Pastor, R. W.; Brooks, B. R. *J. Chem. Phys.* **1995**, *103*, 4613–4621.
(46) Moore, P. B.; Lopez, C. F.; Klein, M. L. *Biophys. J.* **2001**, *81*, 2484–2494.
(47) Yeh, I.-C.; Hummer, G. *J. Phys. Chem. B* **2004**, *108*, 15873–15879.
(48) de Oliveira, C.; Hamelberg, D.; McCammon, J. *J. Chem. Phys.* **2007**, *127*, 175105.
(49) Hamelberg, D.; Shen, T.; McCammon, J. A. *J. Chem. Phys.* **2006**, *125*, 094905.
(50) Johnson, Q.; Doshi, U.; Shen, T.; Hamelberg, D. *J. Chem. Theory Comput.* **2010**, *6*, 2591–2597.
(51) Doshi, U.; Hamelberg, D. *J. Chem. Theory Comput.* **2011**, *7*, 575–581.
(52) Shen, T.; Hamelberg, D. *J. Chem. Phys.* **2008**, *129*, 034103.
(53) Feller, S. E.; Venable, R. M.; Pastor, R. W. *Langmuir* **1997**, *13*, 6555–6561.
(54) Markwick, P.; Cervantes, C.; Abel, B.; Komives, E.; Blackledge, M.; McCammon, J. *J. Am. Chem. Soc.* **2010**, *132*, 1220–1221.
(55) Fajer, M.; Swift, R.; McCammon, J. *J. Comput. Chem.* **2009**, *30*, 1719–1725.
(56) Wereszczynski, J.; McCammon, J. A. *J. Chem. Theory Comput.* **2010**, *6*, 3285–3292.
(57) Davis, P.; Keough, K. *Chem. Phys. Lipids* **1984**, *35*, 299–308.
(58) Curatolo, W.; Sears, B.; Neuringer, L. J. *Biochim. Biophys. Acta Biomembr.* **1985**, *817*, 261–270.